All-Around SiN Stressor for High and Homogeneous Tensile Strain in Germanium Microdisk Cavities

Abdelhamid Ghrib, Moustafa El Kurdi,* Mathias Prost, Sébastien Sauvage, Xavier Checoury, Grégoire Beaudoin, Marc Chaigneau, Razvigor Ossikovski, Isabelle Sagnes, and Philippe Boucaud*

Strain engineering has emerged as a powerful tool to control the properties of electronic and photonic structures. Strain has a direct impact on the mechanical properties and on the material band structures. In electronics, the use of stressor layers is nowadays a standard tool to enhance the transistor carrier mobility in CMOS technology. In photonics, the use of strained semiconductor layers was a very important innovation for emitters to reduce the threshold of semiconductor lasers. More recently, strain engineering has become a key element for silicon photonics.[1] Applying strain can modify the electronic band structures of silicon-based materials as well as the lattice symmetry properties. The centrosymmetry of the silicon lattice can be broken by depositing a stressor layer on top of silicon waveguides thus leading to strain gradient.[2] This feature opens new opportunities for second-order nonlinear processes in silicon-like second harmonic generation, frequency mixing or optical rectification.[3] Another very important field for strain engineering in silicon photonics is the development of a group IV semiconductor laser based on germanium.

Ge is an indirect-band gap material characterized by a small splitting between direct valley (Γ) and indirect valley (L) ≈ 140 meV at room temperature. This splitting can be reduced by introducing tensile strain[4–7] so that for a biaxial tensile strain between 1.7% and 1.9%[5,6] Ge becomes a direct-band-gap.[8,9] Strain is thus the major ingredient to transform an indirect band gap semiconductor into a direct band semiconductor, i.e., turning a poorly efficient semiconductor emitter into an efficient emitter-like III–V semiconductors. There is no need a priori to reach the direct-band gap regime to demonstrate a Ge laser source. The first Ge laser demonstration was obtained with a weak tensile strain around 0.25% resulting from the difference of thermal dilation coefficients between Ge and the silicon substrate.[10,11] This tensile strain amplitude is not sufficient as evidenced by the 300 kA cm^{-2} threshold announced for an electrically pumped laser,[11] a value too high for realistic integration purposes. Enhancing tensile strain transfer into Ge optical cavities is thus requested in order to significantly decrease the lasing threshold, and different approaches have been proposed in the literature.[12–14]

High level strain transfers have been evidenced using strained silicon nitride (SiNH referred to as SiN in the following) layers as stressor layers.[15–20] The use of stressor layers is widely investigated since it relies on a complementary metal oxide semiconductor (CMOS)-compatible process. There are however some trade-offs in strain engineering as evidenced by the link between strain amplitude and cavity volumes, i.e., achieving high tensile strain in large structures being challenging. In this perspective, microdisks are very interesting compact structures as one can expect to transfer high tensile strain and to obtain low lasing threshold due to whispering gallery mode confinement.[21,22] A 1% biaxial strain transfer on the top of a Ge microdisk using strained SiN deposition has been recently demonstrated.[20] One of the drawbacks of this recent demonstration is the spatial inhomogeneity of the transferred strain. This limitation can be lifted by using an all-around stressor method in a similar way that a gate all-around design provides more flexibility to tailor the properties of advanced CMOS transistors.[23]

In this letter, we demonstrate an all-around stressor approach allowing one to reach up to 1.5% biaxial strain on top of Ge microdisks. We show that this all-around stressor approach can combine a high biaxial strain amplitude, a homogeneous in-plane strain and a limited strain gradient across the Ge thickness. The main advantage of this method is to simultaneously strain the top and the bottom of the microdisk by using initially compressively-strained SiN. This strain engineering approach is here demonstrated on Ge structures with the objective to achieve a compact germanium laser source. But the all-around stressor concept goes beyond the simple germanium case and could also stimulate new developments for strained silicon photonics.

We use a 500 nm thick Ge film epitaxially grown on a GaAs substrate. The use of GaAs substrate allows one to overcome

Dr. A. Ghrib, Dr. M. El Kurdi, M. Prost, Dr. S. Sauvage, Prof. X. Checoury, Dr. P. Boucaud
Institut d'Electronique Fondamentale
CNRS-Université Paris Sud
F-91405 Orsay, France
E-mail: abdelhamid.ghrib@u-psud.fr; moustafa.el-kurdi@u-psud.fr

M. Prost
STMicroelectronics
850 rue Jean Monnet 38920 Crolles, France

G. Beaudoin, Dr. I. Sagnes
Laboratoire de Photonique et de Nanostructures
CNRS-UPR 20, Route de Nozay
91460 Marcoussis, France

Dr. M. Chaigneau, Prof. R. Ossikovski
Laboratoire de Physique des Interfaces et des Couches Minces
CNRS, Ecole polytechnique
F-91128 Palaiseau, France

DOI: 10.1002/adom.201400369

 © 2015 WILEY-VCH Verlag GmbH & Co. KGaA, Weinheim

the issue of dislocation density encountered for Ge on Si, thus leading to high quality Ge layers that can be heavily strained.[20] The Ge layer is in situ *n*-doped at around 1×10^{19} cm^{-3}. We first deposit at 300 °C a 250 nm thick compressively strained SiN layer[17] on the whole wafer using a plasma-enhanced chemical vapor deposition (PECVD) process at a pressure of 160 mTorr and with a mixture of SiH_4 and NH_3 gas. We have measured an in-plane stress after deposition of −1.8 GPa in the nitride layer by using the same process on a 4-in.-silicon wafer. The nitride deposition is followed by the deposition of a 800 nm thick SiO_2 layer by PECVD. A 500 nm Au layer is then deposited using evaporating technique on the top of both SiO_2/SiN/Ge/GaAs sample and on a silicon substrate. Both samples are then bonded together using the Au layer as bonding interface at a temperature of 380 °C and an applied bonding pressure of 4 MPa. This process has more than 90% reproducibility. The GaAs substrate is then removed by chemical etching. We have performed e-beam lithography and plasma etching of Ge and buried SiN to define microdisks on the bonded layer. The SiO_2 is selectively under-etched by a buffered hydrofluoric acid solution. At this stage, the initially compressive SiN layer at the bottom stretches the Ge disk. A small delamination of the nitride film, around 100 nm, can be observed at the microdisk edge following this step. It could be reduced by a better selectivity of the etching solution between SiN and SiO_2 (1:12) or by protecting the edges of the microdisk when performing the underetching. A final 300 nm SiN layer deposition step stretches the layer at the top surface. As a result, the Ge disk is entirely buried between two strained SiN layers standing on a SiO_2 pedestal, and we obtain the all-around strained microdisk as shown in **Figure 1**a,b. The SiO_2 layer is used as an optical insulating layer, allowing a vertical gap between the confined optical mode in the germanium layer and the Au layer to avoid optical losses by metallic absorption. We emphasize that this all-around stressor method could also be realized with SiO_2/SiO_2 bonding interface instead of the Au/Au bonding interface used in this work. This would allow integration of strained layers with GOI-like (germanium-on-insulator) technology.

Figure 1c shows a cross-section of the sum of in-plane strain field components ($\varepsilon_r + \varepsilon_\theta$) obtained by finite element modeling (FEM). This modeling considers a hydrostatic initial stress in the SiN of −4.5 GPa that is consistent with the strain transfer measured on micrometer-size structures and a Young modulus of 100 GPa.[17,20] We emphasize that, after relaxation, the stress in the nitride layer differs from this initial value. The strain is homogeneous along the disk diameter except for the decrease at the edge. Figure 1d shows a cross section of the trace of the strain field ($\varepsilon_r + \varepsilon_\theta + \varepsilon_z$). The gain in the structure is linked to the trace component, not to the in-plane components, and we can observe that the trace increases toward the edges. This is a direct consequence of the presence of nitride at the edge of the disk.

We have investigated the strain level at the top of these microdisks using a spatially resolved Raman spectroscopy in a confocal back-scattering configuration.[13,24,25] For these measurements, the laser pump at 532 nm wavelength is focused on the disk surface using a ×100 objective (NA = 0.9). The sample is mounted on a piezo-electric stage allowing an in-plane step displacement of 400 nm. The Raman spectrum is then recorded at each position and is processed to realize the μ-Raman mapping from the disk surface. The shift of the Raman frequency from the unstrained value (≈301.2 cm^{-1}) is proportional to the biaxial strain $\Delta\omega = -b\varepsilon_{//}$ with b = 415 cm^{-1},[26] and $\varepsilon_{//}$ the

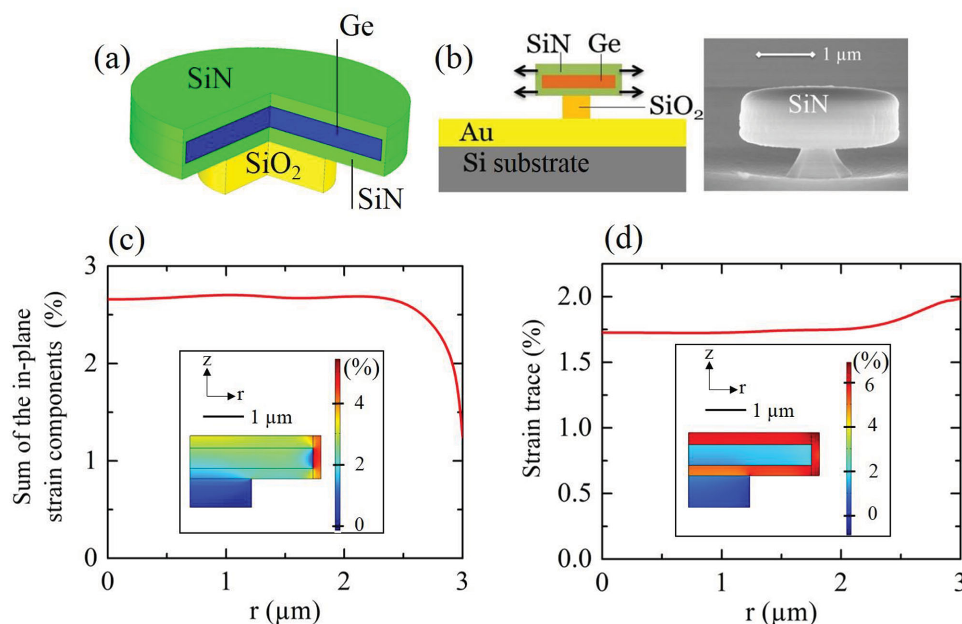

Figure 1. Processing steps leading to all-around-SiN Ge microdisks. a) Schematic view. b) All-around stressed microdisk on a silicon substrate. A corresponding scanning electron microscope image is shown on the right. c) Cross-section along the disk radius of the calculated sum of the in-plane strain components ($\varepsilon_r + \varepsilon_\theta$) 50 nm below the top surface. The sum represents twice the value of the biaxial strain. The inset shows the calculated strain field in the whole structure. d) Cross-section along the disk radius of the calculated trace of the strain components ($\varepsilon_r + \varepsilon_\theta + \varepsilon_z$) 50 nm below the top surface. The inset shows the calculated strain field in the whole structure.

© 2015 WILEY-VCH Verlag GmbH & Co. KGaA, Weinheim

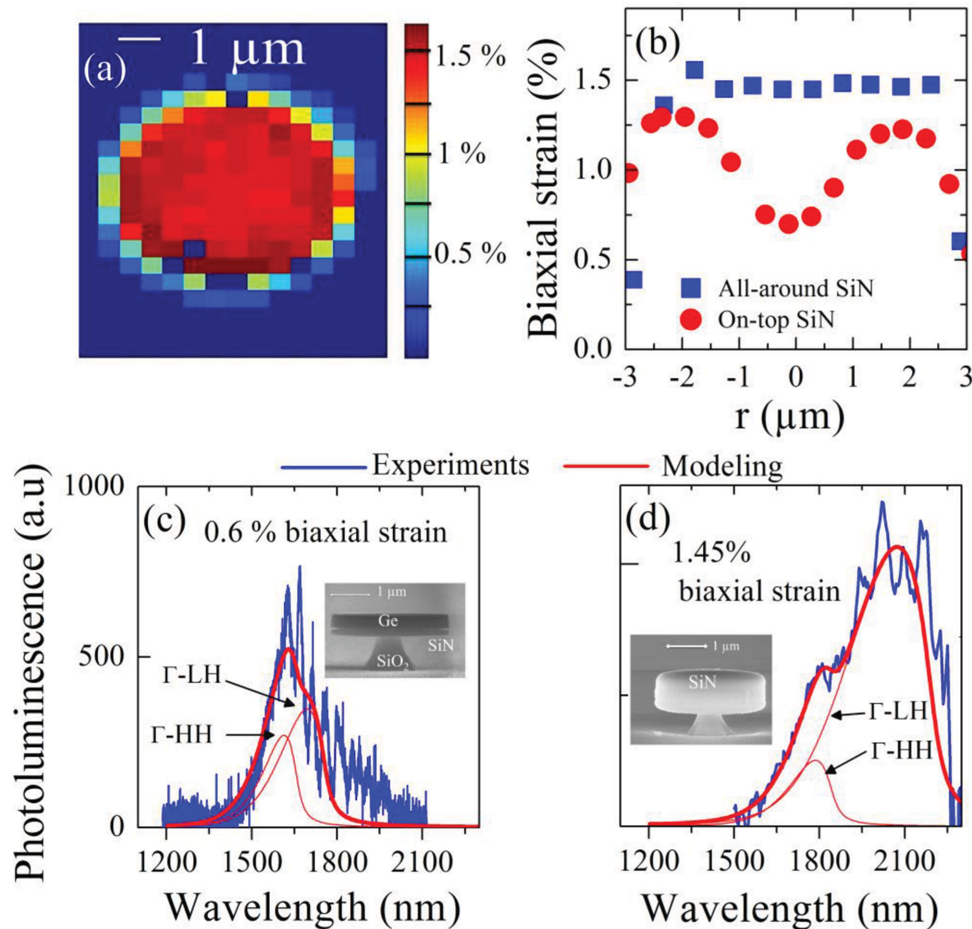

Figure 2. a) Two-dimensional in-plane strain map of the 6 µm diameter all-around SiN microdisk. b) In-plane biaxial tensile strain profile along the disk diameter as deduced from backscattering µ-Raman spectroscopy for 6 µm diameter Ge microdisk. Comparison between a strained microdisk using the on-top only SiN[20] (circles) and an all-around SiN microdisk (squares). c) Photoluminescence spectra of a 6 µm diameter microdisk after SiO_2 under-etching and d) after all-around SiN deposition. Smooth lines correspond to modeling. Thin lines correspond to the contribution of heavy holes (HH) and light holes (LH) bands emission. The modeling does not account for Fabry–Perot resonances.

in-plane biaxial strain. The strain profile is constant at the surface along one disk diameter reaching a biaxial strain value of 1.5% (**Figure 2**a) and only decreases on the last measurement point at the edge. We compare these measurements with those performed on a Ge disk strained by on-top SiN only.[20] In this case, the germanium disk stands directly on a GaAs pedestal. The strain profile is not homogeneous (Figure 2b) showing a minimum of strain of 0.6% at the centre of the microdisk, and reaching ≈1.3% at disk periphery. The Ge disk with an all-around SiN stressor has the advantage to provide an initial stress from the bottom side of Ge leading to a final homogeneous in-plane strain. The decrease of the strain field at the edges, as measured by Raman, agrees with the finite element modeling shown in Figure 1c but we emphasize that it is not detrimental for the germanium gain.

Micro-photoluminescence (µ-PL) measurements were performed in order to estimate the strain at the first stage of strain-transfer. Figure 2c shows the corresponding spectrum. The spectrum signal is modulated by oscillations that we attribute to Fabry-Perot modes resulting from light propagation across the disk diameter.[20] The collected emission is a complex mixing of the direct radiation from the surface and the light scattered from the edge of the disk. It is not possible to unambiguously determinate the contribution of TM and TE polarizations to the emission with our experimental geometry. We have performed the modeling of spontaneous emission using electronic band structures as obtained with a 30 band **k.p** formalism[5] to support the analysis of the photoluminescence results. In this modeling, the calculated amplitude ratio between these transitions results from the joint density of states between conduction band and LH–HH bands and from the calculated carrier distribution in the LH and HH bands. For the first stage of strain–transfer, without SiN on top, the maximum of the emission occurs at 1630 nm and the measured spectrum fits very well with modeling if a biaxial tensile strain of 0.6% is considered. From the FEM analysis we obtain a tensile strain profile across the Ge layer that varies weakly between 0.6% at the SiN/Ge interface (the bottom of Ge disk) and 0.5% at the top surface. Depositing SiN on this structure enhances the red-shift of the spectrum that is a signature of an increase of tensile strain, so that the maximum of the photoluminescence spectrum of the disk is red-shifted toward 2100 nm wavelength (Figure 2d). The

© 2015 WILEY-VCH Verlag GmbH & Co. KGaA, Weinheim

calculated spectrum is in good agreement with the experimental spectrum when 1.45% biaxial tensile strain is introduced in the modeling. This value is in very good agreement with the measured strain from Raman (1.5%) as reported in Figure 2b. For both structures, the contributions of the direct conduction band to light hole (heavy hole) transitions Γ-LH (Γ-HH) are shown in the calculated spectrum. The calculation was performed considering a photogenerated carrier density of 10^{18} cm^{-3} and a doping level $Nd = 10^{19}$ cm^{-3}. As can be seen, the contribution of the Γ-HH transition to the spectrum compared to the Γ-LH transition can differ significantly depending on the level of strain. For the first stage structure (SiN at the bottom only) and the all-around strained structure, the valence band splittings are 45 and 108 meV, respectively. The heavy hole band occupation, and thus the Γ-HH emission, is ruled by strain.

The FEM analysis of the all-around structure predicts 1.37% of tensile strain at the top surface in agreement with the tensile strain measured by Raman (1.5%) and photoluminescence analysis (1.45%). According to modeling, an all-around SiN stressor induces an estimated strain variation of 0.45% from 0.91% at the bottom surface to 1.37% at the top surface (see Figure S1, Supporting Information). In the case of the top-only strained microdisk, the strain variation reaches 0.8% across the Ge layer with a maximum of 1.1% strain at the top and a minimum of 0.3% at the bottom of the layer. An all-around SiN stressor improves the vertical homogeneity and the level of applied tensile strain.

Strain inhomogeneity has an impact on modal gain. In fact, a high strain gradient across the Ge layer limits the modal gain as the overlap between the region with positive gain and optical mode is reduced. We have performed modal gain modeling to evaluate the impact of inhomogeneous strain across the layer. We note that the gain modeling in tensile-strained germanium including the effect of strain inhomogeneity has not been addressed to our knowledge (more details concerning the modeling are presented in the Supporting Information section).

Figure 3a shows the net gain profile calculated at 1900 nm wavelength for TM polarization assuming the strain distributions across the germanium layer for both cases, on-top SiN and

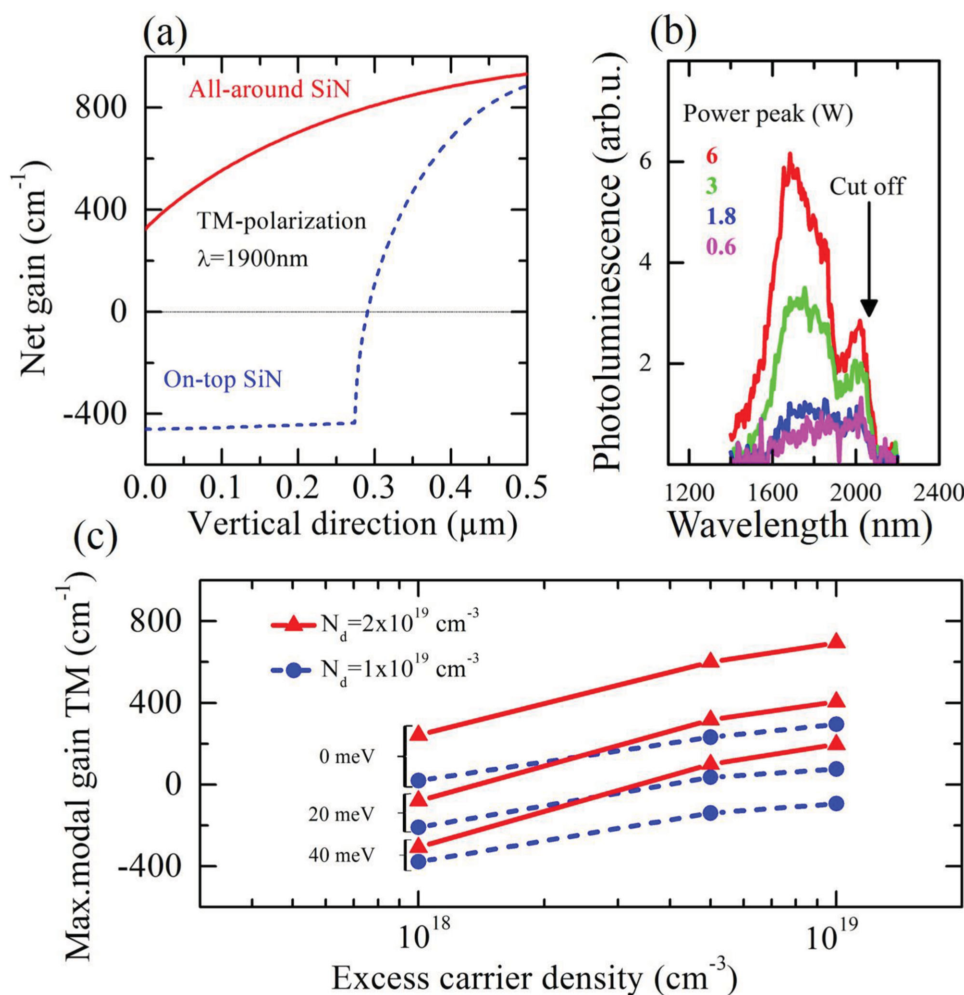

Figure 3. a) Gain modeling along the vertical direction of the Ge layer calculated assuming 1×10^{19} cm^{-3} excess carrier density and 2×10^{19} cm^{-3} doping density for an on-top SiN stressor germanium microdisk[20] (dashed blue line) and an all-around SiN stressor germanium microdisk (red line). b) Experimental photoluminescence spectrum of the all-around stressed microdisk under pulsed pumping for different pump powers (see Supporting Information for details). c) Dependence of the maximum net modal gain with excess carrier density for different doping levels (N_d) calculated using Equation (S2) (Supporting Information), without homogenous broadening and using Equation (S3) (Supporting Information) for a broadening Γ_0 of 20 and 40 meV.

© 2015 WILEY-VCH Verlag GmbH & Co. KGaA, Weinheim

all-around SiN. A doping density of 2×10^{19} cm^{-3} and an injection level of 1×10^{19} cm^{-3} were considered for this calculated profile. It can be seen that the on-top only SiN structure exhibits an inhomogeneous gain region, with a positive gain value on the last 200 nm while the rest of the layer is absorbing. On the contrary, the gain is positive across the whole layer for the all-around structure. The modal gain difference between the two structures is pronounced with a total net modal gain value of –41 cm^{-1} at disk centre (+17 cm^{-1} 300 nm from the edge) for the on-top only case while a positive gain value of 700 cm^{-1} at disk centre (970 cm^{-1} 300 nm from the edge) is found for the all-around strained structures. Note that a whispering gallery mode with $n = 1$ radial number has a field maximum at about 300 nm from the edge. For a doping of 1×10^{19} cm^{-3} and an injection of 1×10^{19} cm^{-3}, the modal gain for the all-around strained structures reaches 300 cm^{-1} (Figure 3c). A variation of ≈–40% of the modal gain values at 300 nm from the edge is estimated if we take into account the delamination of the nitride film at the back surface. These results are obtained for a gain calculation that does not account for homogeneous broadening of the optical transition following Equation (S2), Supporting Information.

Figure 3b shows the measurements of the disk emission under high pumping power by using a pulsed laser diode (see also Figure S4, Supporting Information). We observe the band filling effect in the heavy hole band under high pumping power, leading to a strong blue-shift of the emission. As discussed in the Supporting Information section, we deduce from this measurement that we are able to achieve carrier injection larger than 10^{19} cm^{-3}. Despite such high injection level we find no evidence of gain in the microdisk, while the modeling predicts hundreds of cm^{-1} of positive gain. In previous works,[6] gain in tensile-strained and n-doped germanium were mostly calculated without including the homogeneous broadening of the optical transition. In these studies hundreds of cm^{-1} of gain were also predicted. The more realistic approach is to take into account the broadening following Equation (S3), Supporting Information. The broadening is an important factor that depends on intrinsic parameters and extrinsic parameters like doping or photoinduced carrier density.[27] Enhanced electron scattering rates with impurities and electron–electron interaction rates are expected when very high carrier densities are involved leading to a shortening of the dephasing times. To highlight the influence of the broadening on the gain calculation, we have performed the calculation with various values that can reasonably be considered at room temperature for an n-doped material. In Figure 3c we summarize the results of the maximum net modal gain obtained with the all-around structure using Equation (S2) without broadening (Supporting Information) and using Equation (S3) (Supporting Information) with a homogeneous broadening of 20 meV ($T_2 \approx 65$ fs) and 40 meV. It is clear that the maximum achievable gain is strongly diminished or can be completely inverted to absorption when broadening is taken into account. There is no gain for the 40 meV broadening for a 1×10^{19} cm^{-3} doping level, giving an explanation for the absence of experimental gain in the present structure. The gain for a doping level of 2×10^{19} cm^{-3} is more robust. The increase of germanium doping, which seems to be the most successful way to achieve high gain in strained germanium, has thus some important drawbacks as it decreases minority carrier lifetime and increases homogeneous broadening.

In conclusion, an all-around stressor approach has been proposed and applied to germanium microcavities. This all-around method offers more flexibility to engineer the tensile strain and adjust the strain amplitude and spatial homogeneity. The interest of the method is demonstrated in the case of germanium microdisk cavities but could be applied to other geometries. We expect that reducing germanium thickness down to 300 nm would enhance the transferred strain to even higher values than 1.5% biaxial strain. We have shown that it is mandatory to take into account a realistic value of homogeneous broadening in order to properly estimate the gain in n-doped germanium. Thus, the quantitative evaluation of the homogeneous linewidth of the direct band gap transition needs to be investigated in more details.

Supporting Information

Supporting Information is available from the Wiley Online Library or from the author.

Acknowledgements

This work was supported by Triangle de la Physique under Gerlas convention and by Agence Nationale de la Recherche under GRAAL convention (ANR Blanc call 2011 BS03 00401). This work was also in part supported by the RENATECH network and by CNano-Région Ile de France NANOETCH project. Mathias Prost is funded by a CIFRE grant with the support of STMicroelectronics.

Received: August 21, 2014
Revised: October 28, 2014
Published online: January 2, 2015

[1] C. Schriever, C. Bohley, J. Schilling, R. B. Wehrspohn, *Materials* **2012**, *5*, 889.
[2] R. S. Jacobsen, K. N. Andersen, P. I. Borel, J. Fage-Pedersen, L. H. Frandsen, O. Hansen, M. Kristensen, A. V Lavrinenko, G. Moulin, H. Ou, C. Peucheret, B. Zsigri, A. Bjarklev, *Nature* **2006**, *441*, 199.
[3] M. Cazzanelli, F. Bianco, E. Borga, G. Pucker, M. Ghulinyan, E. Degoli, E. Luppi, V. Véniard, S. Ossicini, D. Modotto, S. Wabnitz, R. Pierobon, L. Pavesi, *Nat. Mater.* **2012**, *11*, 148.
[4] P. H. Lim, S. Park, Y. Ishikawa, K. Wada, *Opt. Express* **2009**, *17*, 16358.
[5] M. El Kurdi, G. Fishman, S. Sauvage, P. Boucaud, *J. Appl. Phys.* **2010**, *107*, 013710.
[6] M. Virgilio, C. L. Manganelli, G. Grosso, G. Pizzi, G. Capellini, *Phys. Rev. B* **2013**, *87*, 235313.
[7] M. V. Fischetti, S. E. Laux, *J. Appl. Phys.* **1996**, *80*, 2234.
[8] J. R. Sánchez-Pérez, C. Boztug, F. Chen, F. F. Sudradjat, D. M. Paskiewicz, R. B. Jacobson, M. G. Lagally, R. Paiella, *Proc. Natl. Acad. Sci. U.S.A.* **2011**, *108*, 18893.
[9] C. Boztug, J. R. Sánchez-Pérez, F. F. Sudradjat, R. B. Jacobson, D. M. Paskiewicz, M. G. Lagally, R. Paiella, *Small* **2013**, *9*, 622.
[10] J. Liu, X. Sun, R. Camacho-Aguilera, L. C. Kimerling, J. Michel, *Opt. Lett.* **2010**, *35*, 679.
[11] R. E. Camacho-Aguilera, Y. Cai, N. Patel, J. T. Bessette, M. Romagnoli, L. C. Kimerling, J. Michel, *Opt. Express* **2012**, *20*, 11316.

© 2015 WILEY-VCH Verlag GmbH & Co. KGaA, Weinheim

[12] M. J. Süess, R. Geiger, R. A. Minamisawa, G. Schiefler, J. Frigerio, D. Chrastina, G. Isella, R. Spolenak, J. Faist, H. Sigg, *Nat. Photonics* **2013**, *7*, 466.
[13] P. Boucaud, M. El Kurdi, A. Ghrib, M. Prost, M. de Kersauson, S. Sauvage, F. Aniel, X. Checoury, G. Beaudoin, L. Largeau, I. Sagnes, G. Ndong, M. Chaigneau, R. Ossikovski, *Photonics Res.* **2013**, *1*, 102.
[14] C. Boztug, J. R. Sánchez-Pérez, J. Yin, M. G. Lagally, R. Paiella, *Appl. Phys. Lett.* **2013**, *103*, 201114.
[15] G. Capellini, G. Kozlowski, Y. Yamamoto, M. Lisker, C. Wenger, G. Niu, P. Zaumseil, B. Tillack, A. Ghrib, M. de Kersauson, M. El Kurdi, P. Boucaud, T. Schroeder, *J. Appl. Phys.* **2013**, *113*, 013513.
[16] M. de Kersauson, M. El Kurdi, S. David, X. Checoury, G. Fishman, S. Sauvage, R. Jakomin, G. Beaudoin, I. Sagnes, P. Boucaud, *Opt. Express* **2011**, *19*, 17925.
[17] A. Ghrib, M. de Kersauson, M. El Kurdi, R. Jakomin, G. Beaudoin, S. Sauvage, G. Fishman, G. Ndong, M. Chaigneau, R. Ossikovski, I. Sagnes, P. Boucaud, *Appl. Phys. Lett.* **2012**, *100*, 201104.
[18] G. Capellini, C. Reich, S. Guha, Y. Yamamoto, M. Lisker, M. Virgilio, A. Ghrib, M. El Kurdi, P. Boucaud, B. Tillack, T. Schroeder, *Opt. Express* **2014**, *22*, 399.
[19] D. Nam, D. Sukhdeo, S.-L. Cheng, A. Roy, K. Chih-Yao Huang, M. Brongersma, Y. Nishi, K. Saraswat, *Appl. Phys. Lett.* **2012**, *100*, 131112.
[20] A. Ghrib, M. El Kurdi, M. de Kersauson, M. Prost, S. Sauvage, X. Checoury, G. Beaudoin, I. Sagnes, P. Boucaud, *Appl. Phys. Lett.* **2013**, *102*, 221112.
[21] J. Van Campenhout, P. Rojo Romeo, P. Regreny, C. Seassal, D. Van Thourhout, S. Verstuyft, L. Di Cioccio, J.-M. Fedeli, C. Lagahe, R. Baets, *Opt. Express* **2007**, *15*, 6744.
[22] T. Baba, D. Sano, *IEEE J. Sel. Top. Quantum Electron.* **2003**, *9*, 1340.
[23] S. Bangsaruntip, G. M. Cohen, A. Majumdar, Y. Zhang, S. U. Engelmann, N. C. M. Fuller, L. M. Gignac, S. Mittal, J. S. Newbury, M. Guillorn, T. Barwicz, L. Sekaric, M. M. Frank, J. W. Sleight, *IEEE Int. Electron Devices Meet.* **2009**, DOI 10.1109/IEDM.2009.5424364
[24] I. De Wolf, *Semicond. Sci. Technol.* **1996**, *11*, 139.
[25] M. J. Süess, R. A. Minamisawa, R. Geiger, K. K. Bourdelle, H. Sigg, R. Spolenak, *Nano Lett.* **2014**, *14*, 1249.
[26] Y. Bai, K. E. Lee, C. Cheng, M. L. Lee, E. A. Fitzgerald, *J. Appl. Phys.* **2008**, *104*, 084518.
[27] W. W. Chow, S. W. Koch, *Semiconductor-Laser Fundamentals*, Springer-Verlag, Berlin, Heidelberg **1999**.

© 2015 WILEY-VCH Verlag GmbH & Co. KGaA, Weinheim